Ceramics International 50 (2024) 39226–39234

Contents lists available at ScienceDirect

Ceramics International

journal homepage: www.elsevier.com/locate/ceramint

Design and magnetron sputtering of nanomultilayered W_2N/Ag-SiN_x films: Microstructural insights and optimized self-lubricant properties from room temperature to 500 °C

Jing Luan [a,b,1], Fanlin Kong [a,1], Manuel Evaristo [b,c], Filipe Fernandes [b,c,d], Yazhou Zhou [e], Albano Cavaleiro [b,c], Hongbo Ju [a,b,c,f,g,*]

[a] School of Materials Science and Engineering, Jiangsu University of Science and Technology, Mengxi Road 2, Zhenjiang, Jiangsu Province, 212003, China
[b] University of Coimbra, CEMMPRE, Department of Mechanical Engineering, Rua Luís Reis Santos, 3030-788, Coimbra, Portugal
[c] University of Coimbra, ARISE, Department of Mechanical Engineering, Rua Luís Reis Santos, 3030-788, Coimbra, Portugal
[d] CIDEM, ISEP - Polytechnic of Porto, Rua Dr. António Bernardino de Almeida, 4249-015, Porto, Portugal
[e] Max Planck Institute for Polymer Research, Mainz, 55128, Germany
[f] Weifang University, School of Machinery and Automation, Laboratory for Sustainable Surface Engineering of Agricultural Machinery Systems, Dongfeng Road 5147, Weifang, Shandong Province, 261061, China
[g] University of Ljubljana, Faculty of Mechanical Engineering, TINT - Laboratory for Tribology and Interface Nanotechnology, Aškerčeva 6, 1000 Ljubljana, Slovenia

ARTICLE INFO

Keywords:
Magnetron sputtering
W_2N/Ag-SiN_x multilayered films
Ag-SiN_x layer thickness
Mechanical properties
Tribological properties

ABSTRACT

Novel multilayered films were engineered by integrating W_2N and Ag-SiN_x layers in a multilayer structure to obtain improved hardness and tribological properties. The films were fabricated by alternating magnetron sputtering, depositing 40 nm layers of W_2N with varying thickness of Ag-SiN_x layers varying in thickness from 4 to 20 nm. The effect of the increase thickness of the Ag-SiN_x layers in the films microstructure and tribological properties were accessed. Tribological experiments were conducted at room temperature (RT), 500 °C, and RT-500 °C cycling conditions. The results revealed the production of a multilayered structure comprising single fcc-W_2N layers interspersed with dual-phase layers consisting of fcc-Ag and amorphous SiN_x phases. Tribological results indicated an improvement in the tribological performance with increase thickness of the Ag-SiN_x layer up to 12 nm. The tribo-synergistic/combined action of both W_2N and Ag-SiN_x layers, along with the presence of layered lubricant tribo-phases of WO_3 and Ag_2WO_4, showcased the pivot role in reducing friction and enhancing wear resistance. The optimized multilayered film, featuring a 12 nm Ag-SiN_x layer, demonstrated exceptional tribological properties under temperature-cycling from RT to 500 °C.

1. Introduction

Achieving sustainable production and development is a monumental challenge nowadays industries, necessitating harmonization between the economy, society, and environment [1]. The utilization of new materials in moving parts to decrease friction and wear, in the absence of harmful liquid lubrication, e.g. engineering bearings and piston rings, is of urgent needed these days [2,3].

Classical high-temperature self-lubricant nitride-based films, i.e. Mo_2N, W_2N, and VN, etc., have been widely developed over the last decades, taking advantage of the formation of the low friction tribo-phases, named as Magneli phases, in the sliding contact [4–6]. The wide temperature range self-lubricant properties were further improved by doping these nitrides with an optimized content of soft metals (SMe, i.e. Ag, Cu), inducing so-called tribological adaptive behaviors [7–10]. For instance, P. Ren et al. [11] was able to improve the tribological properties of the VN films with addition of ~15 at.% of Ag. Henceforth, numerous self-lubricant TMN-SMe systems were designed and developed for achieving relatively low friction coefficients in a wide range of temperatures [12–19]. However, the fast diffusion of the soft metal towards the wear track surface at high temperature easily resulted in the premature failure of the coatings and consequently, to the depletion of

* Corresponding author. School of Materials Science and Engineering, Jiangsu University of Science and Technology, Mengxi Road 2, Zhenjiang, Jiangsu Province, 212003, China.
E-mail addresses: hbju@just.edu.cn, hju@uc.pt (H. Ju).
[1] The co-first authors.

https://doi.org/10.1016/j.ceramint.2024.07.292
Received 21 May 2024; Received in revised form 7 July 2024; Accepted 19 July 2024
Available online 20 July 2024

the lubricious phase. This have been hindering the transfer of those low friction solutions to real industrial components [20]. Recently the use of anti-diffusion barrier layers such as protective SiN_x [21,22], have shown to mitigate and even stop the rapid diffusion of soft metals to the surface. While the protective layers effectively hinder the dispersion of lubricant phases, thus offering enhanced durability, it inevitably entails a trade-off, compromising the inherent lubricant efficacy of the films.

The key challenge to design and produce long-term self-lubricant films consists on the combination of the following merits:(i) the tribo-oxidation of both TMN matrix and SMe additive agent to form optimized content of the low friction tribo-layer, for maintaining the low friction coefficient in a wide range of temperatures; (ii) anti-diffusion of the lubricant agents towards to the surface, for the long-term lubricant behaviors.

In our previous research, tribological results conducted at SiN_x films (matrix) with optimized content of Ag additions to prove an effective improvement of the wear resistance at room and middle temperatures, due to the control release of the lubricious phase [23–26]. The low-release of the lubricant agents promoted by the SiN_x was also confirmed by Mo_2N–Ag/SiN_x multilayered systems [24].

In this paper, W_2N and Ag-SiN_x, with optimized properties [25,26], were selected for modulation layers, and multilayered films altering layers of W_2N and Ag-SiN_x were produced for developing self-lubricant solutions over a wide range of temperatures. The embedding Ag into the amorphous SiN_x will allow to upgrading the wear-resistance performance through avoiding Ag outwards diffusion. The optimized content of each agent in the multilayered films by changing the thickness of the modulation layers, will allow to long-term tribological behavior through the potential formation of the lubricant tribo-layers in a wide range of temperatures. Accordingly, W_2N/Ag-SiN_x multilayered films with different period thickness were produced via reactive magnetron sputtering, employing a sequential deposition process of W_2N and Ag-SiN_x layers. The multilayer films were produced keeping a constant thickness of the W_2N layer (~40 nm), whilst, the thickness of the Ag-SiN_x layer was varied within the range of 4–20 nm. The influence of the period layer thickness on their tribological performance was meticulously examined at different testing temperatures/conditions (room temperature, 500 °C, and RT-500 °C cycling conditions).

2. Experimental part

2.1. Film deposition

A series of multilayered W_2N/Ag-SiN_x films, with varying period thickness trough the change of the thickness of the Ag-SiN_x layer, were deposited using reactive DC magnetron sputtering, using the separated high-purity targets of tungsten (99.8 %), silver (99.9 %) and silicon (99.7 %) with a size of 80 × 80 × 5 mm (the schematic depiction of the deposition machine is shown in the graphic abstract). The designed films were deposited on two types of substrates polished mirror finished high-speed $W_{18}Cr_4V$ (W18) and Si (100) wafers. Before the deposition, the substrates underwent ultrasonic cleaning in acetone for 15 min followed by alcohol for another 15 min. Subsequently, they were placed inside the chamber in a substrate holder, maintaining a distance of 75 mm form the targets. The base pressure in the chamber was below 1.0×10^{-5} Pa. To enhance adhesion of the films to the substrate, a gradient interlayer from pure W to WN_x was firstly deposited at a pressure of 0.5 Pa. This involved depositing a pure W layer with a thickness around 100 nm using a single W target powered with 150 W in a pure Ar environment with a gas flow of 100 sccm for 15 min. Then, N_2 gas was gradually introduced from 0 to 3 sccm at a rate of 0.15 sccm/min to deposit the gradient WN_x layer for 20 min. Subsequently, the multilayered film was fabricated by switching the shutter in front of the W and (Ag + Si) targets. The depositions were conducted under a gas mixture of Ar + N_2, with an Ar/N_2 ratio of 10/3. During the deposition, 200, 250 and 50 W of power was set to the W, Ag, and Si targets, respectively. The thickness of the W_2N layer was maintained at approximately 40 nm by controlling the shutter opening time for the W target, while the thickness of the Ag-SiN_x layer was varied to 4, 8, 16, 12, and 20 nm by adjusting the shutter opening time for the targets of Ag and Si. The shutters movement were automatically controlled by the software. No bias was applied to the substrates during the deposition, however, substrate heating was employed to maintain a substrate temperature of 300 °C. Reference W_2N and Ag-SiN_x monolayer films were also deposited under identical parameters for comparison purposes.

2.2. (Micro)structural measurements

The elemental compositions of the monolayer films and consequently the composition of those layers in the multilayer films, were measured by Energy Dispersive Spectrometer (EDS, Bruker, Germany). The crystal phase of the monolayered and multilayered films was investigated by X-ray diffraction (XRD, Shimazu-6000, Shimadzu, Kyoto, Japan) with Cu Kα radiation, covering a 2θ range of 30-80° with a step of 0.4°. The chemical bonding in the monolayer films was investigated by X-ray photoelectron spectroscopy (XPS, ESCALAB250X, USA), calibrated using C1s at 284.8 eV. Before XPS analysis, the sample surface was gently cleaned using Ar^+ ions beam bombardment for 5 min to remove containments. The cross-sectional microstructure of the multilayer film with 4 nm Ag-SiN_x layer was analyzed using a transmission electron microscope (TEM, Tecnai G2 F20, FEI, USA), with an acceleration voltage of 200 kV. Preparation of TEM specimens involved an Ion Beam Thinner system (GATAN 691, GATAN, USA) to achieve a critical thickness.

2.3. Mechanical and tribological measurements

A nano-indentation system (Anton Paar, CPX + NHT2+MST, Switzerland) was employed to assess the hardness and reduce elastic modulus of the specimens. A load of 3 mN and a holding time of 10 s was used on the experiments. 15 measurements were performed in two different zones of the specimens to ensure the accuracy of the results. Wear tests were conducted under various condition including room temperature (RT), 500 °C, and RT-500 °C cycling conditions using a pin-on-disc wear tester (RTEC, USA). Alumina balls with a diameter of 10 mm served as the counterpart. The RT and 500 °C tests were conducted in open air with the following parameters: (i) rotation speed of 50 rpm, (ii) applied load of 3 N, (iii) testing time of 20 min, (iv) radius of the wear track of 4 mm. The relative humidity during the RT wear test was approximately 30 %. The optimized multilayer film exhibiting the lowest friction coefficient and wear rate at both RT to 500 °C was selected for test the temperature-cycling tribological testing. This involved subjecting the specimen to a sequential temperature cycles from RT to 500 °C. Specially, the specimen was initially subjected to RT tribological testing for 10 min, using the same parameters as referred above for RT test (referred to as RT-1 in the discussion part), followed by 10 min of 500 °C testing at the same wear track under the similar parameters (referred to as 500-1). This temperature-cycling tribo-testing was repeated five times. After the wear tests, the average friction coefficient of the films was determined from the steady-state zone of their corresponding friction curves. The wear tracks were analyzed using a 3D Profiler (BRUKER, Dektak-XT, Germany) to obtain 2D profiles, and the wear rate was calculated using Archard's law. Optical microscope, as well as Raman spectroscopy (inVia, Renishaw, UK) were employed for further characterization of the wear tracks.

3. Results and discussion

3.1. Microstructure

The content of W, N and O in the W_2N monolayer film is 68.9 ± 3.5, 27.3 ± 1.3 and 3.8 ± 0.1 at.%, respectively. This stoichiometry aligns

with previous reports on binary W–N films deposited by magnetron sputtering [27,28]. The Ag-SiN_x monolayered film contains 15.8 ± 1.0 at.% Ag, 40.3 ± 1.3 at.% Si, 41.1 ± 1.3 at.% N, and 2.8 ± 0.1 at.% O. This Ag concentration was selected based on our prior investigations [29].

Fig. 1 depicts the XRD diffraction patterns of the W_2N, Ag-SiN_x monolayer films, as well as the W_2N/Ag-SiN_x multilayered films. The W_2N monolayer film exhibits five diffraction peaks at ~36, ~42, ~62, ~75 and ~78°, assigned to the fcc-W_2N phase for (111), (200), (220), (311), and (222) plans, respectively. Five diffraction peaks can be observed in the XRD diffraction patterns of the monolayer Ag-SiN_x film. Four of the peaks can be assigned to fcc-Ag phase, and the one located at ~70° corresponds to the signal from the Si wafer substrate. No diffraction peaks referring to SiN_x can be detected, in good agreement with the literature reports SiN_x phase presents an amorphous character [30]. The XRD patterns of the W_2N/Ag-SiN_x multilayered films, regardless of the Ag-SiN_x layer thickness, show five diffraction peaks, assigned to fcc-W_2N. A shoulder peak of low intensity at ~38° can also be detected, corresponding to the signal fcc-Ag (111).

The XPS spectra of the monolayer films are depicted in Fig. 2. As shown in Fig. 2(a), the W 4f XPS spectra of the W_2N monolayer film reveal prominent peaks at approximately 35.8, and 38 eV, indicative of W–N bonds [31]. The less intensity peaks at approximately 32.3 and 33.2 eV corresponding to W–O bonds [32]. This confirms the predominant phase of W_2N in the W_2N monolayer. The N 1s spectrum of the W_2N film (Fig. 2(b)) exhibits a peak at 400.8 eV, corresponding to W–N bonds [33]. The O 1s spectrum, as shown in Fig. 2(c), displays peaks at ~ 531 eV and 532.3 eV, attributable to W–O [34] and W–N–O bonds [35], respectively. The XPS spectrum of the Ag-SiN_x monolayered film, shown in Fig. 2(d) illustrates peaks at about 368 and 374 eV in the Ag 3d spectrum, both corresponding to Ag–Ag bonds [24,36,37]. The XPS peaks located at 99, 101 eV and 97,103 eV, are assigned to Si–N [38,39] and Si–O [40] bonds, respectively, in Fig. 2(e). Fig. 2(f) displays N 1s spectrum with peaks at ~397.2 and 398.1 eV, corresponding to Si–N [10,16,26] and Si–O–N [41] bonds, respectively. As for the O 1s spectra, there is a peak at 531 eV corresponding to Si–O bond [42] and another peak located at about 532.6 eV corresponding to Si–O–N bond [43]. Analysis of both monolayer film XPS results confirms W_2N as the primary phase in the W_2N film, while Ag and SiN_x coexist as the main phases in the Ag-SiN_x film. The amorphous nature of SiN_x is supported

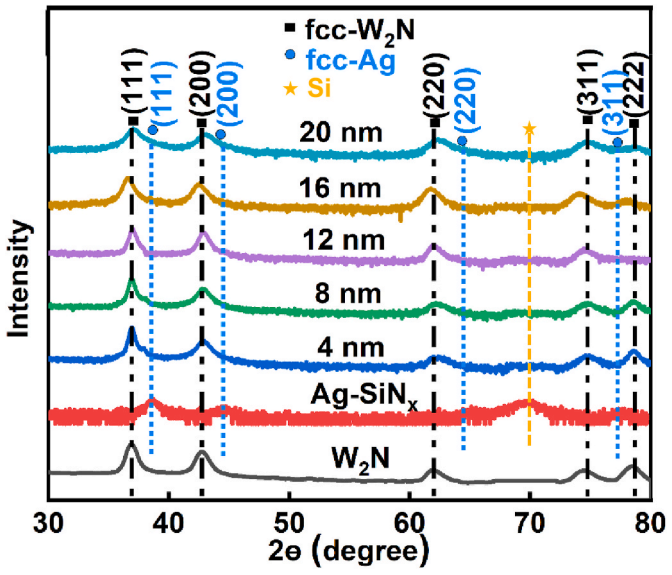

Fig. 1. XRD diffraction patterns of W_2N/Ag-SiN_x multilayered films with different Ag-SiN_x layer thickness, as well as the reference W_2N, Ag-SiN_x monolayer films.

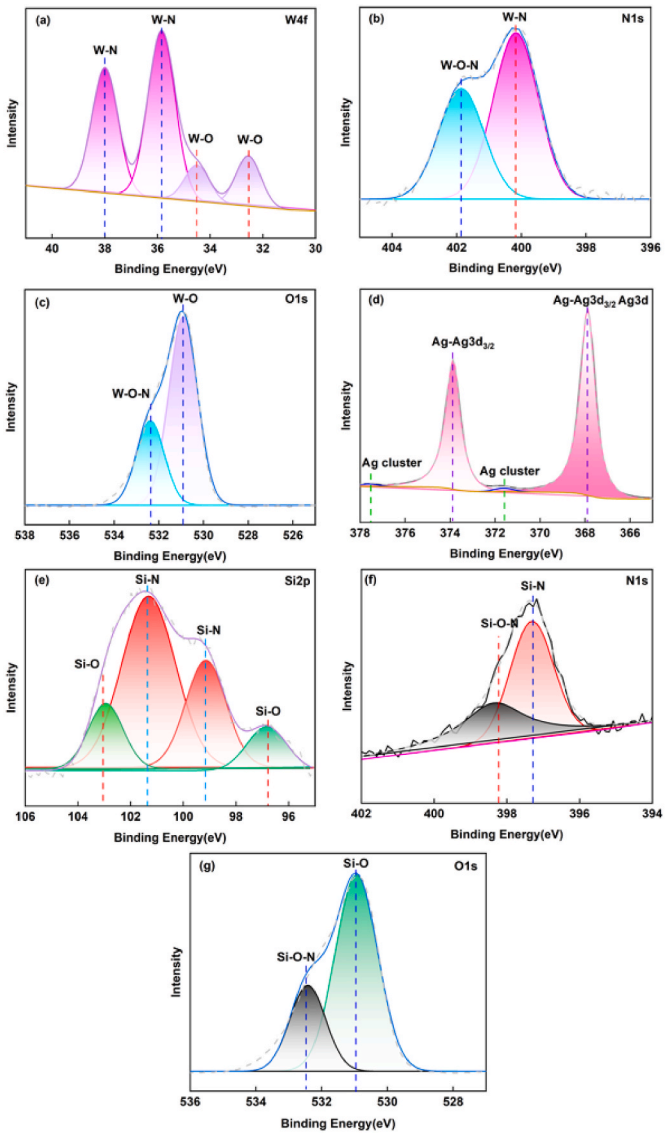

Fig. 2. XPS spectra of reference monolayered films: W_2N film (a) W 4p, (b) N 1s, (c) O 1s; and Ag-SiN_x film (d) Ag 3d, (e) Si 2p, (f) N 1s, (g) O 1s.

by the absence of discernible diffraction peaks in the XRD pattern.

The cross-sectional TEM results of the multilayered film with the 4 nm Ag-SiN_x layer is presented in Fig. 3. Fig. 3(a) illustrates the multilayer architecture of the films where can be distinguish the W_2N (dark layers) and Ag-SiN_x (light layers) layers. The corresponding selected area electron diffraction (SEAD) pattern, shown in the inset of Fig. 3(a), reveals two kinds of diffraction rings corresponding to fcc-W_2N and fcc-Ag, respectively. Fig. 3(b) provides a high-magnification TEM image of the cross-sectional multilayer film, with measured thickness of approximately 40 nm for W_2N layer and 4 nm for Ag-SiN_x layer, consistent with predictions. The interfaces between adjacent modulation layers are discernible in this figure. Additionally, Fig. 3(b) displays the elemental map distribution of W, Ag, and Si from the zone A, corresponding to a zone where both W_2N and Ag-SiN_x layers can be observed. Darker particles within the Ag-SiN_x layer, according to the elemental map distribution, corresponds to Ag nano-particles, The presence of Ag nanoparticles within the amorphous SiN_x matrix is attributed to the extremely low solid solubility of Ag in SiN_x and poor wettability of Ag on the ceramic SiN_x matrix [44]. Fig. 3(c) depicts the HRTEM image of the multilayered film, revealing numerous visible stacking faults within the W_2N layer. The inverse fast Fourier transform (IFFT) image from zone B

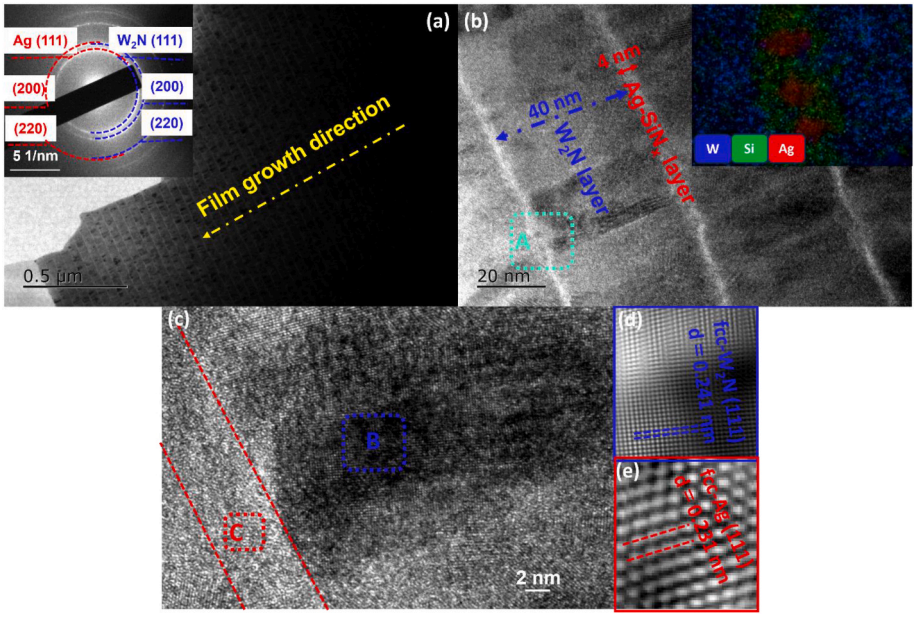

Fig. 3. TEM results of the cross-sectional W_2N/Ag-SiN_x multilayered film with 4 nm Ag-SiN_x layer: (a) the cross-sectional TEM image and its SAED pattern in insert, (b) TEM image with higher magnification and the W, Si, Ag elements mapping from region A, (c) HRTEM image of the cross-sectional multilayered, and (d) IFFT pattern from region B and (e) interplanar spacing from region C.

in Fig. 3(d) displays lattice fringes with a lot of dislocations, with a spacing of approximately 0.241 nm, consistent with fcc-W_2N (111) planes. The Ag-SiN_x layer exhibits the co-existence of amorphous and crystalline phases, as evident in the lighter and thinner layer shown in Fig. 3(c). IFFT image from the nano-crystalline (zone C) and its interplanar spacing is shown in Fig. 3(d) and (e) which can be indexed as belonging to the fcc-Ag(111) planes. Notably, no visible epitaxy growing between Ag/SiNx and W_2N could be detected in the HRTEM image, despite of such feature be reported for other coating systems, e.g. TiN/SiN_x [45], Mo_2N/SiN_x [46], Mo_2N-SiN_x/Ag-SiN_x [47]. This absence is attributed to: (i) the Ag-SiN_x layer thickness surpass a critical value, as SiN_x epitaxial growth with the crystal nitride template is limited to below 1 nm [48,49]; (ii) embedding of Ag nano-particles within the amorphous matrix precludes coherent structure formation with the W_2N template, despite the minimal lattice mismatch between fcc-W_2N (111) and fcc-Ag (111) planes; (iii) It is challenging for the W_2N layers with poor crystalline quality (Fig. 3(c)) to provide a suitable interface for forming a coherent structure, where Ag can epitaxially grow on the W_2N template.

Based on the comprehensive analysis conducted through XRD, XPS and TEM, the monolayer film of W_2N demonstrates a distinct single-phase of fcc-W_2N. On the other hand, the Ag-SiN_x monolayer film manifests a dual-phase composition, comprising fcc-Ag and amorphous SiN_x. In the multilayer film, characterized by varying thicknesses of Ag-SiN_x layers, a pronounced interface between each adjacent modulation layer is evident. Notably, the W_2N layers exhibit a singular fcc-W_2N phase replete with dislocations, while, the Ag-SiN_x layers shows a dual-phase structure comprising amorphous SiN_x and embedded Ag nano-particles disturbed within the amorphous matrix.

3.2. Hardness and elastic modulus

The hardness and elastic modulus of the multilayer films as a function of the Ag-SiN_x layer thickness are presented in Fig. 4. The hardness and elastic modulus of the monolayer W_2N and Ag-SiN_x films deposited as reference are also represented in the same figure, being approximately 26 and 11 GPa, and 388 and 180 GPa. The hardness and elastic modulus of the multilayered film with lower period thickness is slight lower that for reference monolithic W_2N film. Despite of the multilayer

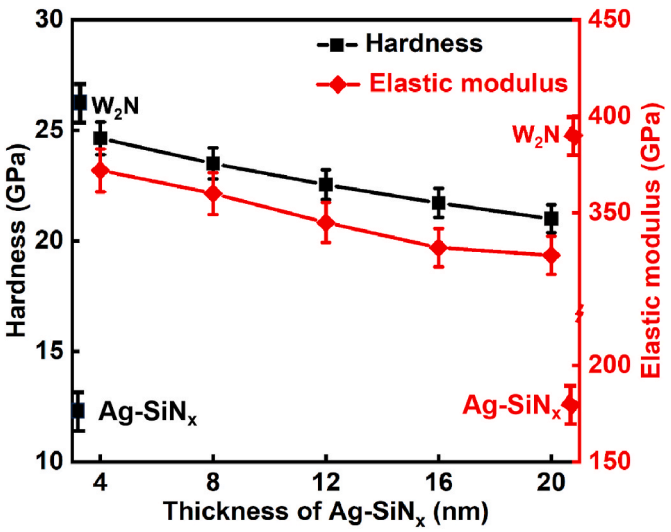

Fig. 4. The hardness and elastic modulus of the W_2N/Ag-SiN_x multilayered films with different Ag-SiN_x layer thickness, as well as its reference W_2N, Ag-SiN_x monolayered film.

structure produced the superlative effect was not able to be reached and a lower hardness was achieved due to the presence of the Ag-SiN_x layers which displays a very low hardness as compared to Ag-SiN_x. As the thickness of the Ag-SiN_x layer increases, both the hardness and elastic modulus of the multilayer films displayed a gradual decline, due to the increase amount of the soft Ag-SiN_x phase.

3.3. Tribological performance

3.3.1. Room and high temperature tribological performances

The average friction coefficient (COF) and wear rate (WR) of the multilayer and monolithic films, at room temperature (RT) and 500 °C, are summarized in Table 1. At RT, the W_2N monolayer film exhibits a COF of approximately 0.41 and a WR of about 7.3×10^{-8} mm^3/N.mm. However, the film was worn out at 500 °C. For the Ag-SiN_x monolayer

Table 1
Average friction coefficient and wear rate of the W_2N, Ag-SiN_x monolayer film and the W_2N/Ag-SiN_x multilayered films with different Ag-SiN_x layer thickness, after the tribo-testing at room temperature (RT) and 500 °C.

The film system	Average friction coefficient		Wear rate (mm^3/N.mm)	
	RT	500 °C	RT	500 °C
W_2N monolayer film	0.41	/	$(7.3 \pm 0.5) \times 10^{-8}$	/
Ag-SiN_x monolayer film	0.35	0.63	$(3.1 \pm 0.5) \times 10^{-6}$	$(4.1 \pm 0.5) \times 10^{-6}$
multilayer film at 4 nm Ag-SiN_x	0.41	0.36	$(6.9 \pm 0.5) \times 10^{-8}$	$(2.8 \pm 0.5) \times 10^{-6}$
multilayer film at 8 nm Ag-SiN_x	0.36	0.24	$(1.3 \pm 0.5) \times 10^{-8}$	$(7.5 \pm 0.5) \times 10^{-7}$
multilayer film at 12 nm Ag-SiN_x	0.30	0.22	$(9.3 \pm 0.5) \times 10^{-9}$	$(2.1 \pm 0.5) \times 10^{-7}$
multilayer film at 16 nm Ag-SiN_x	0.35	0.23	$(2.3 \pm 0.5) \times 10^{-8}$	$(7.4 \pm 0.5) \times 10^{-7}$
multilayer film at 20 nm Ag-SiN_x	0.38	0.34	$(8.9 \pm 0.5) \times 10^{-8}$	$(1.3 \pm 0.5) \times 10^{-6}$

film, the COF at RT is approximately 0.35 with a corresponding WR of about 3.1×10^{-6} mm^3/N.mm. At 500 °C, the COF increases to around 0.63 with a WR of approximately 4.1×10^{-6} mm^3/N.mm. The COF of the Ag-SiN_x multilayer film with the lower period thickness at RT is similar to that of the W_2N reference film; however, it gradually decreases to approximately 0.30 with increasing Ag-SiN_x layer thickness up to 12 nm. An inverse trend is then observed, with the COF increasing to about 0.38 for a 20 nm Ag-SiN_x layer thickness. A parallel trend is noted in the WR, initially decreasing with increasing Ag-SiN_x layer thickness, reaching a minimum value of approximately 9.3×10^{-9} mm^3/N.mm for the 12 nm Ag-SiN_x layer, then showing an upward trend. This trend aligns with the evolution of the COF values. At 500 °C, the COF values of the films are always lower than when compared to the RT ones, and much lower that the Ag-SiN_x monolayer film with a COF of 0.36, decreasing for around 0.22 for the multilayer film with 12 nm Ag-SiN_x layer thickness, followed by a further gradual increase. A similar variation trend is observed for the WR at 500 °C, with the lowest value achieved at approximately 2.1×10^{-7} mm^3/N.mm for the 12 nm Ag-SiN_x thickness. Based on the previous results, it seems that the multilayer film with 12 nm of the Ag-SiN_x layer displayed the best compromise between WR and COF, at both RT and 500 °C.

Fig. 5 shows the wear track morphology of selected multilayer films after tribological testing at RT and 500 °C. The RT wear track of the film with 12 nm Ag-SiN_x layer is shown in Fig. 5(a). A very smooth surface could be observed, except a scratch on the center of the wear track, which could be caused by the hard debris moving along the counterpart: the asperities was easily broken from the film under the applied load as well as the induced shear stress, when it was contacted by the counterpart during the sliding. The movement of the counterpart with drag the hard particle among the wear debris over the surface of the film producing a fine screech. Higher number of scratches are visible for the multilayer film with 20 nm Ag-SiN_x layer thickness, and a wider wear track is formed, as shown in Fig. 5(b). The elevated SiN_x content with increased Ag-SiN_x layer thickness enhances the likelihood of abrasive wear, due to its brittle but hard nature. Additionally, the dropping of the hardness degrades the load-carrying ability and, consequently, leads to an expanded wear track width. The darker coloration at the center of the wear track suggests complex tribo-chemical interactions with atmospheric oxygen/moisture during the sliding (Raman results shown latter supports this affirmation, in Fig. 6).

F ig. 5(c)and (d) depicts the morphology of the wear track at 500 °C for the multilayer films with 12 and 20 nm of the Ag-SiN_x layer. A significant accumulation of dark wear debris is evident on both sides of the wear track, accompanied by the presence of fine scratches in the central area of the wear track. Compared with Fig. 5(c) and (d) demonstrates that increasing the thickness of the Ag-SiN_x layer results in: (i) the near disappearance of the dark wear debris, (ii) a notable increase in fine scratches, (iii) the expansion of the wear track width. The elevated SiN_x content in the overall multilayer films with the increased Ag-SiN_x layer thickness attributes to above results, due to its high thermal stability, and mechanical characteristics of hard but brittle.

The Raman spectra obtained from the wear track of the multilayer films for both RT and 500 °C tests, as a function of the layer thickness are depicted in Fig. 6. Regardless of the thickness of the Ag-SiN_x layer, the Raman spectra from the RT wear tests reveal a prominent peak at approximately 150 cm^{-1} bands, corresponding to the W_2N phase [50], which is consistent with previously studies on PVD sputtered W_2N films [51]. Additionally, minor Raman peaks with low intensity, observed around 280, 330, and 800 cm^{-1}, could be indexed to the presence of WO_3 phase [52]. The Raman peak with very weak intensity, positioned at aproximatly1000 cm^{-1} could be indexed to the Ag_2WO_4 phase [53]. The presence of such phases on the wear tracks have been seen beneficial in enhancing the anti-frictional properties at room temperatures [54].

At 500 °C, a distinct tribo-phase, Ag_2WO_4, emerges in the spectra for both multilayer films with 12 and 20 nm Ag-SiN_x layer thickness, as per

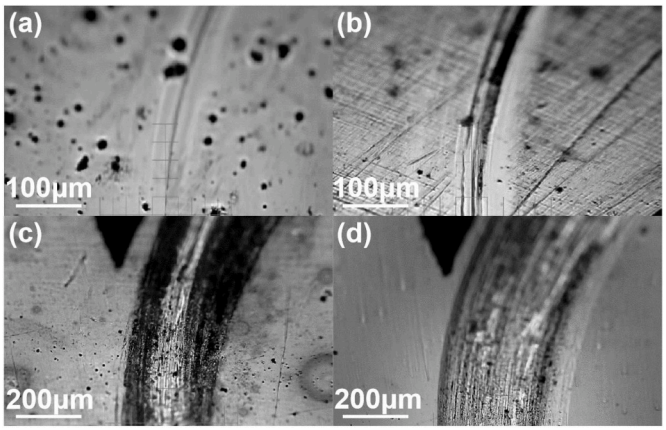

Fig. 5. The optical image of the multilayered film's wear track: (a) 12 nm Ag-SiN_x layer at RT, (b) 20 nm Ag-SiN_x layer at RT, (c) 12 nm Ag-SiN_x layer at 500 °C, (d) 20 nm Ag-SiN_x layer at 500 °C.

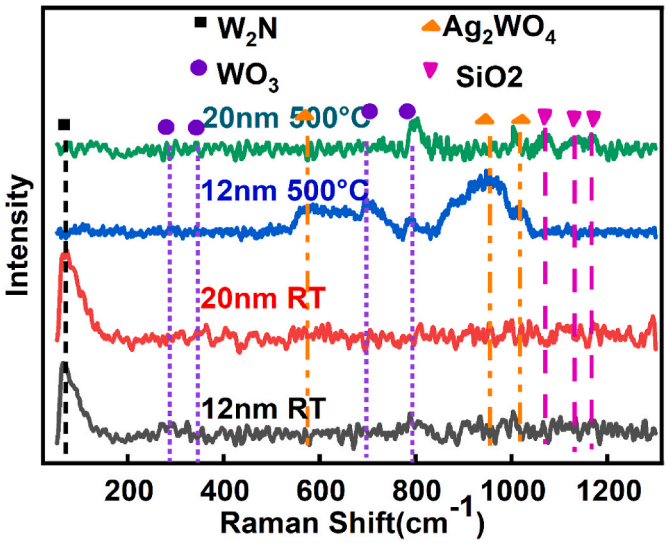

Fig. 6. The wear track Raman spectrum of the multilayered film with various Ag-SiN_x layer thickness from both RT and 500 °C.

previous Raman peak information [53]. The intensity of the WO_3 peaks at 500 °C notably surpasses that observed at RT, indicating higher quantity of tribo-phase formation under higher temperatures. Furthermore, the intensity of SiO_2 Raman peaks increases with the thickness of the Ag-SiN_x layer, suggesting a higher content of SiO_2 with thicker Ag-SiN_x layers.

Some tungsten suboxides, known as Magneli phases (denoted by the formulas W_nO_{3n-1} and W_nO_{3n-2}) are esteemed for their self-lubricating properties, particularly in high-temperature tribological scenarios [55]. These materials, due to their layered structure, have been identified as effective lubricants, exhibiting remarkable friction-reducing properties in various environments. Additionally, bimetallic oxides have been explored as lubricating friction phases, leveraging their layered compositions for superior tribological performance. In a comprehensive investigation by Stone et al. [53], the high-temperature friction properties of Ag_2WO_4 phase were meticulously investigated by both simulations and experimental characterizations. The results confirmed a good self-lubricant performance of Ag_2WO_4 phase, evidenced by a gradual reduction in the COF from 0.56 at RT to 0.43 at 600 °C, employing Si_3N_4 as the friction pair. Furthermore, it was also observed that the thermal decomposition of tungstate ternary oxide phases could facilitate the formation of Ag cluster, thereby, also significantly contributing to the improving self-lubricant properties due to the low friction properties of this kind of material. Thus, the presence of tribo-phases of Ag, WO_3 and Ag_2WO_4, showcase the potential to reduce both friction and wear in multilayered W_2N/Ag-SiN_x films.

Based on the comprehensive tribo-testing results outlined above, a notable finding is the lower RT COF observed for the Ag-SiN_x monolayer film compared to that of the W_2N monolayer one. This observation underscores the potential of inserting the Ag-SiN_x layer into the W_2N matrix to enhance its anti-frictional properties through the multilayered architecture. As the thickness of the Ag-SiN_x layer increases, a corresponding decrease in COF is observed, with the multilayer film reaching its minimum COF value of approximately 0.30 at an Ag-SiN_x layer thickness of 12 nm. Indeed, it is noteworthy that this COF value is even lower than those recorded for both reference monolayer films. This is crucial to acknowledge the significant role played by the synergistic tribological interaction between the layers of W_2N and Ag-SiN_x, which promotes the formation of bimetallic oxides such as Ag_2WO_4. This mechanism substantially contributes to the improvement of the anti-friction properties of the multilayer film, leading to a further reduction in COF. The augmented lubricant capacity contributes to an improvement in WR.

Nevertheless, there is a gradual increase in both COF and WR at RT with a further increment in the thickness of the Ag-SiN_x layer. The primary factors contributing to the deterioration of anti-frictional properties may stem from the augmented relative content of the hard tribo-phase SiO_2 within the wear track. This is accentuated by thicker Ag-SiN_x layers, resulting in more pronounced scratches as it moves along the counterpart (Fig. 5). The heightened frictional force consequently leads to higher COF values. Additionally, factors such as low hardness, expanded contact area with the counterpart, contribute to the decline in wear resistance.

At 500 °C, the multilayer films displayed even lower COF values than at RT due to the presence of the lubricant agents of Ag, WO_3 and Ag_2WO_4. It should be noted that at high temperature the formation of oxides is facilitated. Furthermore, the gradual increase in the relative content of Ag, an elevated temperature lubricant agent, with increasing Ag-SiN_x layer thickness further bolsters the improvement in tribological properties. Nevertheless, an escalation in the thickness of the Ag-SiN_x layer beyond 12 nm precipitates a decline in both COF and WR at 500 °C. The principle contributing factors encompass: (i) the heightened relative content of SiN_x, characterized by exceptional thermal stability, which effectively curtails tribo-oxidation and impedes the formation of lubricant tribo-phases (as evidenced by Raman spectra), thereby progressively elevating COF. (ii) The SiN_x phase, though brittle yet robust, readily fragments to generate hard wear debris, yielding additional SiO_2 tribo-phase and, consequently instigating more scratch formation, thus undermining both anti-frictional and wear-resistant properties.

3.3.2. Temperature-cycling tribological performance

The W_2N/Ag-SiN_x multilayered film with 12 nm Ag-SiN_x layer thickness, was selected to evaluate their tribological properties under temperature-cycling conditions from room temperature to 500 °C (RT-500-RT-500 …). The friction curves and average friction coefficient are presented in Fig. 7.

An evident running-in period and a steady stage can be observed in the friction curve of the RT-1 tribo-testing. During the running-in stage, the counterpart will contact the surface of the film breaking the asperities and giving variations of the COF value. Even during the steady stage, the friction coefficient exhibits an undulatory behavior, ranging from around 0.20 to about 0.70. this suggests that 600 s tribo-testing is insufficient for achieving full dynamic equilibrium. A relatively stable friction coefficient is reached for 500-1 testing after a sharp drop at the beginning of the testing, from approximately 0.62 to around 0.20 within 120 s. This drop is attributed to the formation of lubricant tribo-phases at 500 °C.

The RT-2 curve exhibits different characteristics of RT-1, showing a gradual rise in the friction coefficient with increased testing time, reaching around 0.82 at the end of this testing. The lubricant tribo-phase generated during 500-1 testing is considered the main factor in maintaining a low friction coefficient at the beginning of RT-2 testing. However, RT tribo-testing lacks the capacity to continuously provide sufficient lubricant tribo-phase, as evidenced by the comparison of RT and 500 °C Raman results (Figs. 6 and 9). As a result, there is a gradual increase in the friction coefficient as a function of testing time during this tribo-testing. It is worth noting that the evaporation of moisture from the environment, coupled with the degradation of the lubricant agents absorbed on the film surface after 500-1 tribo-testing, also contributes to this gradual rise in the friction coefficient. Subsequently, a similar curve to 500-1 is observed under the 500-2 tribo-testing, with an initial gradual decrease in the friction coefficient followed by stability with increased testing time. The main influential factors for 500-1 are still applicable to explain the friction curve tendency in 500-2.

In the third cycle, although a notable undulatory friction curve persists regardless the RT-3 tribo-testing, the gradual increase in coefficient diminishes with the testing time. this could be related to the relative content of lubricant tribo-phases on the wear track. It is also confirmed by the Raman results (Fig. 9). A stable friction coefficient, consistently approximately 0.20, is observed irrespective of testing time or temperature in subsequent cycles, indicating a distinct lubricant mechanism as compared to the previous third cycles.

The average friction coefficient (COF) values shown in Fig. 7 b) also reveals that under RT, as a gradual decrease on COF is observed with the number of cycles, from approximately 0.32 at RT-1 to 0.22 at RT-4, remaining stable after that. However, at 500 °C the COF remains stable at around 0.20 regardless of the number of cycles.

Fig. 8 illustrates the 2D wear track profiles and the corresponding wear rates for the temperature-cycling tribo-testing.

After the RT-1 tribo-testing, an evident wear track with a depth and width of about 1 and 250 μm, respectively, is observed, with pronounced scratches on the sides of the wear track. The presence of hard debris on the contact film/ball is the cause for formation of the fine scratches. The subsequent 500-1 tribo-testing increases the width of the wear track to about twice its initial value, with fine scratches still visible on the surface. Additionally, noticeable accumulation of wear debris on both sides of the track is observed, indicating significant wear degradation due to the tribo-oxidation and the formation of layered lubricant tribo-phases, as confirmed by Raman spectroscopy (Figs. 6 and 9).

In the second cycle, the wear track depth significantly increases after the RT-2 tribo-testing, while the width remains almost unchanged compared to that of 500-1. The absence of wear debris accumulation on

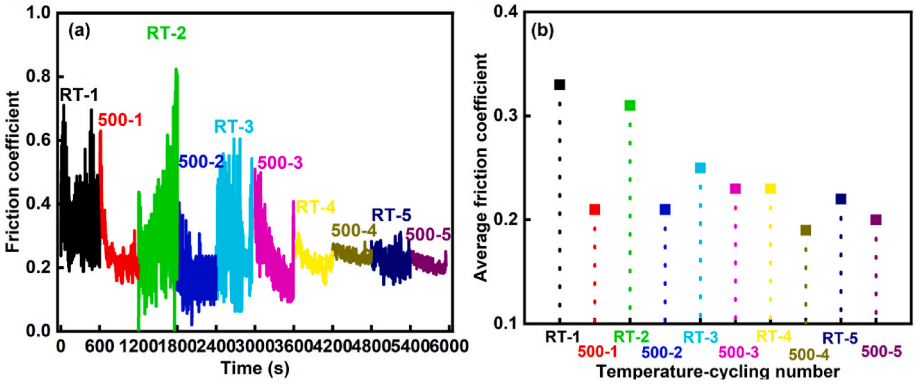

Fig. 7. The friction curves (a) and average friction coefficient (b) corresponding to the multilayer film with a 12 nm Ag-SiN_x layer after the wear test under the five cycles of room temperature to 500 °C (RT-500).

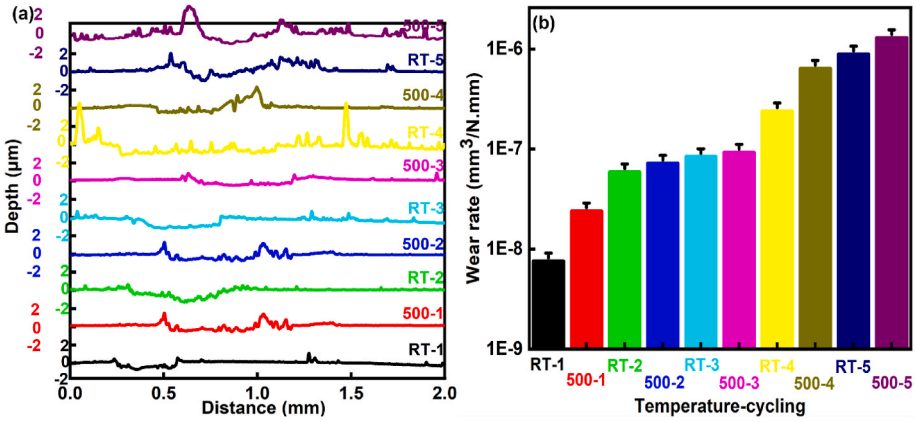

Fig. 8. The 2D wear track morphology (a) and wear rate (b) corresponding to the multilayer film with a 12 nm Ag-SiN_x layer after the wear test under the five cycles of room temperature to 500 °C (RT-500).

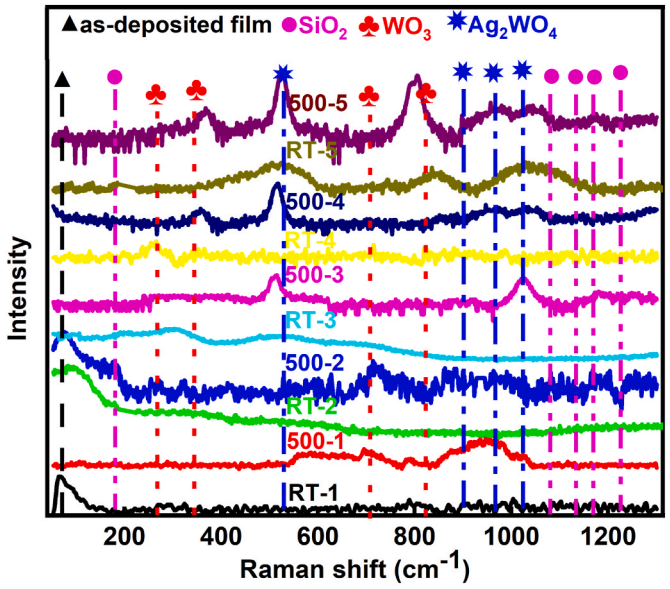

Fig. 9. The Raman spectra from the wear track of the multilayer film with a 12 nm Ag-SiN_x layer following the tribo-testing under the five cycles of room temperature to 500 °C (RT-500).

both sides indicates the abrasive wear type, induced by the counterpart, leading to a notable increase in the wear rate. During the 500-2 wear testing, the depth of the wear track decreases, while the width remains consistent at around 500 μm. This is attributed to volume expansion induced by oxidation at 500 °C, coupled with the accumulation of wear debris adhering to the track surface.

Following the RT-3 tribo-testing, the wear track exhibits a relatively smooth morphology with no evident presence of wear debris accumulation on both sides, suggesting polishing wear as the primary wear mechanism, which results in the consumption of the tribo-layers and a softening of the interaction between the film and counterpart. Consequently, this slight increases the depth and width compared to those observed under the 500-2 conditions. However, an expansion in the wear track is evident for the 500-3 cycle, indicating an increase in the WR.

Following the morphological evaluation, there is a noticeable trend of increasing depth in the wear track with each cycle, along with a consistent accumulation of wear debris on both sides of the tracks during the subsequent two cycles. Notably, even after the 500-5 cycle tribo-testing, the maximum depth of the wear track remains below the thickness of the film. This observation suggests that the film retains the capacity to work effectively under the same demanding temperature-cycling conditions.

The WR of the multilayered film, presents three distinct stages: (i) a notable increase of the WR from RT-1 to RT-2, (ii) a slight increase in WR value from RT-2 to RT-3, and (iii) a significant increase in WR from 500 to 3 to 500-5.

Fig. 9 presents the Raman spectra obtained from the wear track of the multilayer film following the wear test after undergoing five cycles of

RT-500. The Raman spectrum obtained from the wear track during the RT-1 tribo-testing exhibits similar features to those observed during the RT tribo-testing, with a prominent Raman peak at approximately 150 cm^{-1}, indicating the presence of the as-deposited film. Additionally, minor peaks with low intensity at around 280, 330, and 800 cm^{-1}, corresponding to the WO_3 [52], and 1000 cm^{-1}, to Ag_2WO_4 [56]. Following the 500-1 tribo-testing, both the number and intensity of the Raman peaks associated with the tribo-phases increase, suggesting an increase on the amount of these tribo-phases.

However, the Raman spectrum obtained from the wear track during the RT-2 tribo-testing reveals no evident peaks assigned to WO_3, Ag_2WO_4 and SiO_2 phases. This absence of peaks is attributed to the limited formation of tribo-phases, possibly caused by the evaporation of moisture from the environment or absorbed on the surface following the 10-min exposure to the 500 °C environment. Following the 500-2 tribo-testing, evident Raman peaks attributed to the WO_3, SiO_2 and Ag_2WO_4 phases are visible. The formation of these tribo-phases is attributed to tribo-oxidation of the film under the combined action of the testing temperature and frictional heat.

Subsequent to the RT-3 tribo-testing, although Raman peaks corresponding to the tribo-phases are observed, their intensity is lower as compared to those observed during the 500 °C testing. This suggests a decrease in the relative content of the tribo-phases on the wear track, caused by the consumption of tribo-layers during the sliding and the limited capacity to form tribo-phases at RT. However, the Raman spectrum obtained from the 500-3 tribo-testing exhibits obvious peaks corresponding to the tribo-phases, indicating sufficient tribo-phase formation during sliding.

Based on the previous experiments, the temperature-cycling from room temperature to 500 °C has a significant impact on the tribological behaviors of the W_2N/Ag-SiN_x multilayered film: (i) in the first cycle, the lubricant mechanism during the RT-1 tribo-testing is similar to that observed at RT, with the formation of tribo-phases and synergistic/combined actions between the W_2N and Ag-SiN_x layers maintaining a COF of around 0.32, close to the value observed at RT. The tribo-oxidation process occurring during the 500 °C tribo-testing significantly reduces the COF to approximately 0.20, albeit with an increased in WR. (ii) In the subsequent two cycles, a slightly different lubricant mechanism is observed compared to the first cycle. The residual lubricant phase formed during 500-1 continues to lubricate the film during RT-2, maintaining a relatively low COF of around 0.32. However, due to the evaporation of moisture and limited capacity for forming tribo-phases, lubrication decreases, resulting in an elevated WR due to intense interaction between the counterpart and the film. Tribo-phases are reformed during the 500-2 tribo-testing, reducing the COF to approximately 0.20, with tribo-oxidation contributing to a gradual increase in WR. Despite the consumption of layered tribo-phases by the counterpart, remaining lubricant tribo-phases post elevated tribo-testing continue to lubricate the film, keeping the COF under RT-3 lower than that of RT-1 and 2. Tribo-oxidation remains a significant factor for the low COF and increased WR during 500-3. (iii) In the subsequent cycles, an adequate amount of lubricant tribo-phases on the wear track continuously lubricates the film, maintaining COFs at both RT and 500 °C around 0.20. The consumption of layered tribo-phases at RT as well as the tribo-oxidation at 500 °C gradually increase the WR.

All in all, the W_2N/Ag-SiN_x multilayer film with an optimized 12 nm Ag-SiN_x layer demonstrates excellent temperature-cycling tribological properties from RT to 500 °C, retaining its self-lubricant capacity even after undergoing five rigorous cycles of RT-500.

4. Conclusion

In today's environmentally conscious era, the pursuit of advanced self-lubricant films to replace traditional, environmentally harmful lubricants poses a significant challenge. This study addressed this critical issue by developing W_2N/Ag-SiN_x multilayered films for demanding self-lubricant applications. The films were fabricated using magnetron sputtering, alternating W_2N layers, with a fixed thickness of 40 nm, with Ag-SiN_x layers varying in the thicknesses from 4 to 20 nm. The main conclusion that can be taken from this research are.

(1) The multilayer films demonstrated an architecture characterized by alternating layers of W_2N and Ag-SiN_x. The W_2N layers crystallized in the single phase fcc-W_2N, and the Ag-SiN_x layers in a dual-phases of fcc-Ag and amorphous SiN_x.
(2) Both the hardness and elastic modulus of the multilayered film exhibited a gradual decrease with the increase of Ag-SiN_x thickness, ranging from 4 to 20 nm.
(3) The multilayered architecture effectively combines the properties of both W_2N and Ag-SiN_x layers, thereby enhancing their tribological performance at both RT and 500 °C in a synergistic way between the modulation layers. The optimized multilayer film, characterized by a 12 nm Ag-SiN_x layer, demonstrating superior performance with the lowest COF and WR values at both RT and 500 °C.
(4) The multilayer film, optimized with a 12 nm Ag-SiN_x layer, demonstrated exceptional temperature-cycling tribological properties from RT to 500 °C. The RT COF decreased from RT-1 to RT-3, stabilizing around 0.20, while the 500 °C COF remained consistently low at approximately 0.20, albeit with a continuous increase of wear rate over cycling.

Conflict of interest

We declare that we do not have any commercial or associative interest that represents a conflict of interest in connection with the work submitted.

Hongbo Ju on behalf of the all authors.

CRediT authorship contribution statement

Jing Luan: Writing – original draft, Methodology, Investigation, Data curation. **Fanlin Kong:** Writing – original draft, Investigation. **Manuel Evaristo:** Writing – review & editing. **Filipe Fernandes:** Writing – review & editing, Data curation. **Yazhou Zhou:** Methodology. **Albano Cavaleiro:** Writing – review & editing, Supervision. **Hongbo Ju:** Writing – review & editing, Visualization, Supervision, Resources, Project administration, Methodology, Investigation, Funding acquisition, Formal analysis, Data curation, Conceptualization.

Acknowledgement

Supported by the National Natural Science Foundation of China with the number of 52171071 and 51801081, Mount Taishan Scholar Young Expert of Shandong Province of China, Mobility GT project based on the MSCA COFUND SCHEME of EU, national funds through FCT of Portugal – Fundação para a Ciência e a Tecnologia, under a scientific contract of 2021.04115.CEECIND, 2023.06224.CEECIND, and the projects of UIDB/00285/2020, and LA/P/0112/2020. We also thank H. Ju's master student - Hongying Lu for her contributions to the graphic abstract.

References

[1] M. Woydt, The importance of tribology for reducing CO_2 emissions and for sustainability, Wear 474–475 (2021) 203768.
[2] K. Holmberg, A. Erdemir, Influence of tribology on global energy consumption, costs and emissions, Friction 5 (2017) 263–284.
[3] M.K. Hossain, M.H.K. Rubel, M.A. Akbar, M.H. Ahmed, N. Haque, Md F. Rahman, J. Hossain, K.M. Hossain, A review on recent applications and future prospects of rare earth oxides in corrosion and thermal barrier coatings, catalysts, tribological, and environmental sectors, Ceram. Int. 22 (2022) 32588–32612.
[4] C.K. Liu, H.B. Ju, L.H. Yu, J.H. Xu, Y.X. Geng, W.X. He, J.X. Jiao, Tribological properties of Mo_2N films at elevated temperature, Coatings 9 (2019) 734.

[5] D. Javdosank, J. Musil, Z. Soukup, S. Haviar, R. Cerstvy, J. Houska, Tribological properties and oxidation resistance of tungsten and tungsten nitride films at temperature up to 500°C, Tribol. Int. 132 (2019) 211–220.

[6] Q. Cai, S.X. Li, J.B. Pu, Z.B. Cai, X. Lu, Q.F. Cui, L.P. Wang, Effect of multicomponent doping on the structure and tribological properties of VN-based coatings, J. Alloys Compd. 806 (2019) 566–574.

[7] K. Huang, X.Q. Cao, L.G. Kong, Z.B. Lu, G.A. Zhang, Q. Ding, H.T. Hu, Effect of Ag content on friction and wear properties of Ag and V co-doped CrN coatings at 25-700°C, Ceram. Int. 47 (2021) 35021–35028.

[8] H.B. Ju, N. Ding, J.H. Xu, L.H. Yu, Y.X. Geng, F. Ahmed, The tribological behavior of niobium nitride and silver composite films at elevated testing temperatures, Mater. Chem. Phys. 237 (2019) 121840.

[9] C.K. Liu, H.B. Ju, J.H. Xu, L.H. Yu, Z.T. Zhao, Y. Geng, Y. Zhao, Influence of copper on the compositions, microstructure and room and elevated temperature tribological properties of the molybdenum nitride film, Surf. Coating. Technol. 395 (2020) 125811.

[10] H.B. Ju, R. Zhou, S.J. Liu, L.H. Yu, J.H. Xu, Y.X. Geng, Enhancement of the tribological behavior of self-lubricating nanocomposite Mo_2N/Cu films by adding the amorphous SiNx, Surf. Coating. Technol. 423 (2021) 127565.

[11] P. Ren, S.Z. Zhang, J.X. Qiu, X.Y. Yang, W.W. Wang, Y. Li, Y.X. Si, G.G. Wang, M. Wen, Self-lubricating behavior of VN coating catalyzed by solute Ag atom under dry friction and oil lubrication, Surf. Coating. Technol. 409 (2021) 126845.

[12] H.B. Ju, L.H. Yu, D. Yu, I. Assempah, J.H. Xu, Microstructure, mechanical and tribological properties of TiN-Ag films deposited by reactive magnetron sputtering, Vacuum 141 (2017) 82–88.

[13] X. Xu, J.F. Sun, F.H. Su, Z.J. Li, Y.J. Chen, Z.B. Xu, Microstructure and tribological performance of adaptive MoN-Ag nanocomposite coatings with various Ag contents, Wear 488–489 (2022) 204170.

[14] H.B. Ju, J. Luan, J.H. Xu, A. Cavaleiro, M. Evaristo, F. Fernandes, Nano-multilayered ZrN-Ag/Mo-S-N film design for stable anti-frictional performance at a wide range of temperatures, Friction. https://doi.org/10.1007/s40544-024-0943-y.

[15] H. Li, J.L. Li, J. Kong, J.W. Huang, Q.J. Wu, D.S. Xiong, Achieving high toughness and wear resistance for hard TaN-Ag films actuated by Ag, Int. J. Refract. Metals Hard Mater. 111 (2023) 106076.

[16] Y.P. Zhang, Z.Y. Wang, S.H. Zhou, Y. Zhang, Y.F. Dong, A.Y. Wang, P.L. Ke, Synergistic effect of V and Ag diffusion favored the temperature-adaptive tribological behavior of VAlN/Ag multi-layer coating, Tribol. Int. 192 (2024) 109285.

[17] G.S. Wu, F.L. Song, Y.B. Shi, B. Yu, J.B. Pu, Y.X. Wang, Effect of multi-doping on the tribological behavior of MoN(Ag)-based films in a wide temperature range, Mater. Sci. 58 (2023) 3960–3971.

[18] J. Luan, H.Y. Lu, J.H. Xu, F. Fernandes, M. Evaristo, B.Y. Ma, F.X. Xie, A. Cavaleiro, H.B. Ju, Exploring tribological characteristics of ZrN-MoSN composite films fabricated via RF magnetron sputtering: Insights from microstructure and performance analysis, Surface and Coatings Technology 484 (2024) 130813.

[19] Y. Ren, J.H. Jia, X.Q. Cao, G.Z. Zhang, Q. Ding, Effect of Ag content on the microstructure and tribological behaviors of NbN-Ag coatings at elevated temperatures, Vacuum 204 (2022) 111330.

[20] E.Y. Liu, J.H. Zhang, S. Chen, S.M. Du, H.L. Du, H. Cai, L.L. Wang, High temperature negative wear behaviour of VN/Ag composites induced by expansive oxidation reaction, Ceram. Int. 47 (2021) 15901–15909.

[21] B. Zuo, L.H. Yu, J.H. Xu, The new nanocapsule structure and cyclic tribological properties of Mo_2N/Ag/Si_3N_4 nanocomposite film, Ceramics International 49 (2023) 38982–38994.

[22] H.B. Ju, J.L. Guo, L.H. Yu, J.H. Xu, J. Luan, Enhancement of the mechanical and tribological properties of self-lubricant Mo_2N-Ag composite film by adding amorphous SiNx, Ceram. Int. 50 (2024) 8463–8471.

[23] Y.X. He, X.B. Wang, T. Guo, K.W. Gao, X.L. Pang, Crystal interface-enhanced thermal stability of CrAlN/SiN_x multilayer films, Surf. Coating. Technol. 445 (2022) 128725.

[24] H.B. Ju, R. Zhou, J. Luan, L.H. Yu, J.H. Xu, B. Zuo, J.F. Yang, Y.X. Geng, L.J. Zhao, F. Fernandes, Multilayer Mo_2N-Ag/SiN_x films for demanding applications: morphology, structure and temperature-cycling tribological properties, Mater. Des. 223 (2022) 111128.

[25] H.B. Ju, S. He, L.H. Yu, I. Asempah, J.H. Xu, The improvement of oxidation resistance, mechanical and tribological properties of W_2N films by doping silicon, Surf. Coating. Technol. 317 (2017) 158–165.

[26] H.B. Ju, K.H. Huang, J. Luan, Y.X. Geng, J.F. Yang, J.H. Xu, Evaluation under temperature cycling of the tribological properties of Ag-SiNx films for green tribological applications, Ceram. Int. 49 (2023) 30115–30124.

[27] H.B. Ju, R. Zhou, J. Luan, C.S. Kumar, L.H. Yu, J.H. Xu, J.F. Yang, B.W. Zhang, F. Fernandes, Tribological performance under different environments of Ti-C-N composite films for marine wear-resistant parts, Int. J. Miner. Metall. Mater. 30 (2023) 144–155.

[28] L.H. Yu, H.J. Zhao, H.B. Ju, J.H. Xu, Influence of Cu content on the structure, mechanical and tribological properties of W_2N-Cu films, Thin Solid Films 624 (2017) 144–151.

[29] K. Xu, M. Du, L. Hao, J. Mi, Y. Lin, S. Li, J.N. Wang, X.Y. Deng, Optical optimization and thermal stability of SiN/Ag/SiN based transparent heat reflecting coatings, Infrared Phys. Technol. 122 (2022) 1350–4495.

[30] Y.X. He, X.B. Wang, T. Guo, K.W. Gao, X.L. Pang, Effect of interface on oxidation behavior and tribological properties of CrAlN/SiN_x multilayer films, Ceram. Int. 49 (2023) 1369–1380.

[31] R.L. Li, J.P. Tu, C.F. Hong, D.G. Liu, H.L. Sun, Microstructure, mechanical and tribological properties of CrN/W_2N multilayer films deposited by DC magnetron sputtering, Surf. Coating. Technol. 204 (2009) 470–476.

[32] A. Marikutsa, L. Yang, A.N. Kuznetsov, M. Rumyantseva, A. Gaskov, Effect of W-O bonding on gas sensitivity of nanocrystalline Bi_2WO_6 and WO_3, J. Alloys Compd. 856 (2021) 158159.

[33] H.J. Zhao, C.Y. Mu, F.X. Ye, The effect of modulation of period on the mechanical and wear properties of TiAgN/W_2N coatings, Surf. Coating. Technol. 309 (2017) 29–34.

[34] S.H. Wei, S.J. Li, R.M. Wei, S.S. Liu, W.M. Du, Different morphologies of WO_3 and their exposed facets-dependent acetone sensing properties, Sensor. Actuator. B Chem. 329 (2021) 129188.

[35] L.L. Chen, Z.Y. Zhang, M. Lou, K. Xu, L. Wang, F.N. Meng, D. Music, K.K. Chang, High-temperature wear mechanisms of TiNbWN films: role of nanocrystalline oxides formation, Friction 11 (2023) 469–472.

[36] H.B. Ju, F.L. Kong, J.H. Xu, Y.X. Geng, C.K. Zhang, J. Luan, Influence of Ag on the microstructure, mechanical and tribological properties of SiC-Ag composite film deposited by the industrial DC magnetron sputtering system, Vacuum 218 (2023) 112672.

[37] H.B. Ju, L.Y. Xu, J. Luan, Y.X. Geng, J.H. Xu, L.H. Yu, J.F. Yang, F. Fernandes, Enhancement on the hardness and oxidation resistance property of TiN/Ag composite films for high temperature applications by addition of Si, Vacuum 209 (2023) 111752.

[38] I.V. Sterkhova, A.A. Korlyukov, N.F. Lazareva, V.I. Simirnov, Siltranes: relationship between the experimental Si-N dative bond length and its calculated energy according to AIM analysis data, Chem. Phys. 578 (2024) 112153.

[39] C.R. Das, M. Rangwala, A. Ghosh, Effect of Si contents on microstructure and mechanical characteristics of TiAlSiN thin film deposited by HiPIMS using different TiSi target compositions, Surf. Coating. Technol. 476 (2024) 130212.

[40] J.L. Li, R. Wang, Y.X. Wang, L.P. Wang, Anti-oxidant mechanism of TiAlN/SiN decorative films on borosilicate glass by magnetron sputtering, International Journal of Manufactory Technology 96 (2018) 1563–1569.

[41] X. Pessoloes, Y. Landon, M. Mousseigne, W. Rubio, Simulation of the behaviour of CNC machine-tools in three-axis milling of sculptured surfaces, Int. J. Miner. Metall. Mater. 25 (2010) 326–338.

[42] A.S. Siju, S.D. Waigaonkar, Effect of rake surface textures spacing and width on the cutting performance of inserts in dry machining of titanium alloy, Int. J. Miner. Metall. Mater. 18 (2021) 136–159.

[43] K. Balachander, S. Arulkumaran, T. Egawa, Y. Sano, K. Baskar, A comparison on the electrical characteristics of SiO_2, SiON and SiN as the gate insulators for the fabrication of AlGaN/GaN metal-oxide/insulator-semiconductor high-electron mobility-transistors, Jpn. J. Appl. Phys. 44 (2005) 4911.

[44] Y. Hwang, H. Yim, K. Oh, J. Park, S. Kim, H.W. Jang, J.W. Choi, Highly conductive Ag-SiN_x composite thin film anode engineering for transparent battery, Composites Parts B: Engineering 262 (2023) 110829.

[45] V.I. Ivashchenko, S. Veprek, A.S. Argon, P.E.A. Turchi, L. Gorb, F. Hill, J. Leszczynski, First-principles quantum molecular calculations of structural and mechanical properties of TiN/SiN_x heterostructures and the achievable hardness of the nc-TiN/SiN_x nanocomposites, Thin Solid Films 578 (2015) 83–92.

[46] G.J. Zhang, T.X. Fan, T. Wang, H.L. Chen, Microstructure, mechanical and tribological behavior of MoN_x/SiN_x multilayer coatings prepared by magnetron sputtering, Appl. Surf. Sci. 274 (2013) 231–236.

[47] H.B. Ju, J. Luan, Y.P. Wang, A. Bondarev, M. Evaristob, Yaoxiang Geng, J.H. Xu, A. Cavaleiro, F. Fernandes, Mutual promotion on the mechanical and tribological properties of the nacre-like self-lubricant film designed for demanding green tribological applications, Friction 13 (2024) 9440963.

[48] W. Li, P. Liu, Y.S. Zhao, K. Zhang, F.C. Ma, X.K. Liu, X.H. Chen, D.H. He, SiN_x thickness dependent morphology and mechanical properties of CrAlN/SiN_x nanomultilayers, Thin Solid Films 534 (2013) 367–372.

[49] H.B. Ju, M. Athmani, J. Luan, A. AL-Rjoub, A. Cavaleiro, T.B. Yaqub, A. Chala, F. Ferreira, F. Fernandes, Insights into the oxidation resistance mechanism and tribological behaviors of multilayered TiSiN/CrV_xN hard coatings, Int. J. Miner. Metall. Mater. 30 (2023) 2459–2468.

[50] Y.C. Chan, H.W. Chen, Y.Z. Tsai, J.J. Duh, J.W. Lee, Texture, microstructure and anti-wear characteristics in isostructural CrAlSiN/W_2N multilayer coatings, Thin Solid Films 433 (2013) 265–269.

[51] Y. Deng, S.H. Yin, Y. Hong, Y. Wang, Y. Hu, G.P. Zou, T.C. Kuang, K.S. Zhou, Microstructures and properties of novel nanocomposite WN_x coatings deposited by reactive magnetron sputtering, Appl. Surf. Sci. 512 (2020) 145508.

[52] V. Ganbayle, S. Shaikh, S. Mohite, S. Inamadar, A. Bagade, A. Patil, K. Rajpure, Synergistic effects of Pd decoration and substrates on the NO_2 sensing performance of sprayed WO_3 thin films, Chem. Phys. Lett. 814 (2023) 140327.

[53] D. Stone, J. Liu, D.P. Singh, C. Muratore, A.A. Voevodin, S. Mishra, C. Rebholz, Q. Ge, S.M. Aouadi, Layered atomic structures of double oxides for low shear strength at high temperatures, Scripta Mater. 62 (2010) 735–738.

[54] W. Li, P. Liu, P.K. Liaw, Microstructures and properties of high-entropy alloy films and coatings: a review, Materials Research Letters 6 (2018) 199–229.

[55] M. Thalji, G.A.M. Ali, J. Shim, K.F. Chong, Cobalt-doped tungsten suboxides for supercapacitor applications, Chem. Eng. J. 473 (2023) 145341.

[56] Y. Song, W.Y. Xie, C. Yang, D. Wei, X.T. Sud, L. Lia, Lu Wang, J. Wang, Humic acid-assisted synthesis of Ag/Ag_2MoO_4 andAg/Ag_2WO_4 and their highly catalytic reduction ofnitro-and azo-aromatics, J. Mater. Res. Technol. 9 (2020) 5774–5783.